Journal of Crystal Growth 310 (2008) 5058–5062

Contents lists available at ScienceDirect

Journal of Crystal Growth

journal homepage: www.elsevier.com/locate/jcrysgro

Effect of boron incorporation on growth behavior of BGaN/GaN by MOVPE

G. Orsal [a,*], N. Maloufi [b], S. Gautier [a], M. Alnot [c], A.A. Sirenko [d], M. Bouchaour [a], A. Ougazzaden [e]

[a] Laboratoire Matériaux Optiques, Photonique et Systèmes, UMR CNRS 7132, University of Metz and Supelec, 2 rue E. Belin, F-57070 Metz, France
[b] Laboratoire d'Etude des Textures et Application aux Matériaux, UMR CNRS 7078, University of Metz, ISGMP, Ile du Saulcy, F-57045 Metz, France
[c] Laboratoire de Physique des Matériaux, UMR CNRS 7556, Université Henri Poincaré, Bd des aiguillettes B.P. 239, F-54506 Vandoeuvre les Nancy, France
[d] Department of Physics, New Jersey Institute of Technology, Newark, NJ 07102, USA
[e] Georgia Institute of Technology/GTL, UMI 2958 GT-CNRS, 2-3 rue Marconi, 57070 Metz, France

ARTICLE INFO

Available online 19 August 2008

Keywords:
A1. AFM
A1. Boron segregation
A1. Phase separation
A1. SEM
A1. XPS
A3. MOVPE
B1. BGaN

ABSTRACT

In the family of III-nitride compounds, $B_xGa_{1-x}N$ is particularly attractive because it can be lattice matched to AlN or SiC substrates. In this work we studied in detail the relationship between morphology, composition, and boron surface segregation in $B_xGa_{1-x}N$ layers grown on GaN template substrates by MOVPE. Scanning electron microscopy (SEM) and atomic force microscopy (AFM) observations reveal the formation of large polygonal crystallites for the growth regimes with triethylboron (TEB/III) ratios and film thicknesses exceeding the optimum values. XPS measurements demonstrate that the boron content at the surface is higher compared to that in the volume of the film and it increases with the TEB/III ratio and/or the film thickness. From a given surface boron segregation, drastic variations in the film morphology occur and are attributed to phase separation. Our study demonstrates the possibility to grow $B_xGa_{1-x}N$/GaN/sapphire films of a single phase up to $x = 3.6\%$ by reducing the thickness of the BGaN layers.

1. Introduction

Wide bandgap boron nitride films have attracted special attention due to their unique properties such as thermal conductivity, hardness, and excellent chemical stability. Furthermore, the lattice constants of BGaN alloys can be matched to that of SiC or AlN if sufficient boron incorporation into the lattice is achieved. In addition, these materials offer the possibility of using quaternary BAlGaN alloys in the UV spectral range and hence, provide more degrees of freedom in designing optoelectronic device structures for the short wavelength range. However, phase separation has been reported for BGaN limiting the full exploitation of this potentially useful material. Because BN and GaN binary compounds have large structural dissimilarities, it is quite difficult for the $B_xGa_{1-x}N$ alloy to be grown in a broad range of composition. It has been reported that at the typical growth temperature for $B_xGa_{1-x}N$ (about 1000 °C) the phase diagram contains regions of spinodal decomposition or phase separation in the interval of $0.028 < x < 0.995$ [1,2]. The first experimental results reported by Polyakov et al. [3] showed that the highest boron solubility in GaN grown at 1000 °C on sapphire was about 1%. Wei et al. [4] reported single-phase BGaN alloy on AlN/SiC with the highest boron content of 1.5%. Recently, Ougazzaden et al. [5] reported 5% of boron incorporation for thin multilayers of BGaN/GaN. Besides the interest in BGaN materials for the wide bandgap engineering, it can also be used as a substrate for GaN overgrowth. For instance, Akasaka et al. [6] proposed BGaN micro-islands as a novel buffer for the lateral overgrowth process (ELO) to obtain a low threading dislocation density.

In this work we argue for the possibility of growing $B_xGa_{1-x}N$ single phase layers with higher boron content compared to what has been theoretically predicted and, we discuss the possibility to use single phase $B_xGa_{1-x}N$ as a novel buffer layer for the growth of high quality GaN. Our analysis is based on a detailed structural and morphological study of $B_xGa_{1-x}N$ materials grown by MOVPE on GaN templates. We emphasize the relationship between morphology, composition, and boron segregation.

2. Experimental procedure

The $B_xGa_{1-x}N$ thin films were grown in a T-shape MOVPE reactor [7] using 100% nitrogen as a carrier gas. The trimethylgallium (TMGa), triethylboron (TEB), and ammonia (NH_3) were used as precursor sources for Ga, B, and N, respectively. All the growths were performed at 1000 °C on 3.5 μm thick GaN template substrates on sapphire. A 150 nm thick GaN buffer layer was deposited onto the template substrates followed by the growth of BGaN thin films. The molar ratio of TEB in the vapor phase (TEB/III) was varied from 4% to 8% where III is the total number of

* Corresponding author. Tel.: +33 3 87 37 85 40; fax: +33 3 87 37 85 59.
E-mail address: orsal@metz.supelec.fr (G. Orsal).

0022-0248/$ - see front matter © 2008 Elsevier B.V. All rights reserved.
doi:10.1016/j.jcrysgro.2008.08.024

moles of the group-III sources (TMG+TEB). More details on the growth conditions of BGaN can be found in Ref. [5].

The surface morphology was studied by *in situ* reflectometry, scanning electron microscopy (SEM), and atomic force microscopy (AFM). The thickness was measured by cross-sectional SEM.

The surface and the subsurface chemical compositions of the films were deduced from XPS measurements before and after sputtering. Sputtering with argon ions for several minutes was utilized in order to remove 6–10 mono-atomic layers. Broad range and elemental XPS spectra were measured using Al Kα X-ray and Mg Kα X-ray sources to avoid the overlaps with Auger lines. All the spectra were charge-corrected with respect to the C 1 s photoelectron component peak corresponding to adventitious carbon at a binding energy of 285.0 eV. The peak intensity was normalized to experimental conditions (number of scans, accumulation time, etc.) and to atomic sensitivity factors. The chemical composition was calculated from the area under the corresponding peak with the quantitative accuracy better than $\pm 10\%$ for all elements.

The composition of boron in the solid phase of BGaN layers was determined by using X-ray diffraction (XRD). The θ–2θ scans and reciprocal space maps for symmetric (0 0 0 2) and asymmetric ($1\,1\,\bar{2}\,4$) reflections demonstrated complete relaxation of the BGaN layers. The measured lattice mismatch determined from the angular separation between GaN and BGaN diffraction peaks for the (0 0 0 2) reflection was used for the boron composition calculation in the assumption of no residual strain between the film and GaN substrate. Note that the boron content (TEB/III ratio) in the gas phase of 4%, 6%, and 8% is higher than the solid-phase boron composition of 1.7%, 2.7%, and 3.6%, respectively, as determined with the help of the Vegard's law. More details on XRD data analysis of our samples have been reported in Ref. [5].

3. Results and discussion

The surface morphology of BGaN layers has been investigated as a function of TEB/III ratios by *in situ* optical reflectometry. For a given TEB/III ratio, the intensities of the reflectometry peaks (not shown here) are strong and remain unchanged with the thickness increase until a certain optimum thickness has been achieved. After that, the reflectometry signal suddenly drops down to the background noise level. This degradation is related to an enhanced surface roughness which occurs beyond the optimum thickness. This optimum thickness decreases as TEB/III ratio increases.

In order to understand the relationship between TEB/III ratio and optimum thickness, SEM measurements were performed. The surface morphology of the $B_xGa_{1-x}N$ layers changes drastically with the TEB/III ratio and with the layer thickness, as shown in Fig. 1. At 4% TEB/III ratio, the corresponding images (Fig. 1(a) and (b)) show a homogeneous surface composed of a matrix of small crystallites and numerous V-defects. These pits are known to be formed when threading dislocations intersect the epilayer surface. When the TEB/III ratio increases from 4% to 8%, the morphology changes drastically: V-defects are fully covered by small crystallites and large crystallites with polygonal shape appear, as shown in Fig. 1(g) and (h). The thickness of the film plays an important role as well as the TEB/III ratio.

For a TEB/III ratio of 4% ($x = 1.7$), no large crystallites are shown in a broad range of film thicknesses. This composition falls within the stable region, which corresponds to a BGaN single phase of the calculated phase diagram, at the growth temperature of 1000 °C [1,2]. However, for a 1 μm layer one can notice that in addition to the same crystallites as that for the 175 nm layer, some different crystallites emerge upon the surface.

For BGaN thin layers (50 nm) grown with a TEB/III ratio of 6% (Fig. 1(d)), the morphology is similar to that for 4%. We have also

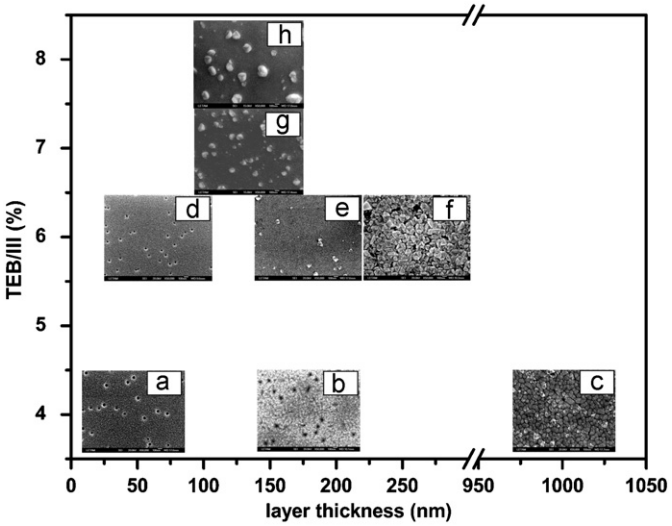

Fig. 1. SEM surface images of $B_xGa_{1-x}N$ of different thicknesses grown with different TEB/III ratios.

investigated by AFM the surface topography of the GaN buffer layer (Fig. 2) and the 50 nm thick overgrowth $B_{0,027}Ga_{0,973}N$ layer (Fig. 3). Hexagonal pits with the high density of $10^9\,cm^{-2}$ appear on the smooth surface of the GaN buffer layer (Fig. 2(a)). These pits are conical in shape with an apparent mean depth of around 25 nm (Fig. 2(b)). AFM surface topography of the overgrowth 50 nm thick $B_{0.027}Ga_{0.973}N$ (TEB/III = 6%) presents small crystallites and less obvious V-defects, as shown in Fig. 3(a). The corresponding cross-sectional AFM scan (Fig. 3(b)) reveals a drastic decrease in pits depth meaning that pits filling is enhanced with thickness. This smooth BGaN layer could be proposed as a buffer for high quality GaN overgrowth with reduced density of threading dislocations.

For a TEB/III ratio of 6%, an increase in the thickness from 50 to 250 nm leads to bury the V-defects and to the formation of large polygonal crystallites. Their size and density increase with the thickness until coalescence and then the full matrix surface coverage, as shown for the 250 nm thick layer (Fig. 1(f)). The mean in-plane size of these polygonal crystallites is about 100 nm and their average height is 56 nm, which results to an RMS surface roughness of around 13 nm deduced from the AFM measurements (Fig. 4). This value is much higher than that of 0.7 nm obtained for the 50 nm layer thickness, i.e. before the formation of large crystallites. These results are in agreement with *in situ* reflectometry measurements from which the signal intensity decreases drastically when the roughness of the surface increases, i.e. the formation of large crystallites upon the surface.

In general, critical thickness for stress relaxation may affect morphology of BGaN film and if the layer thickness exceeds a critical thickness, the morphology can change. Based on XRD data, our BGaN layers are completely relaxed, even for surfaces composed of small crystallites. Thus, we conclude that the change in morphology of our samples is not affected by the critical thickness. Similar modification in the film morphology was observed and attributed by other authors to phase separation [4,6]. In their case, AES analysis gave lower boron content for the large crystallites compared to the surrounding regions (matrix of small crystallites).

According to our previously mentioned results, for a given TEB/III ratio large crystallites appear beyond the optimum thickness. This growth feature, observed for thick films or high TEB/III ratio, could imply that phase separation occurs close

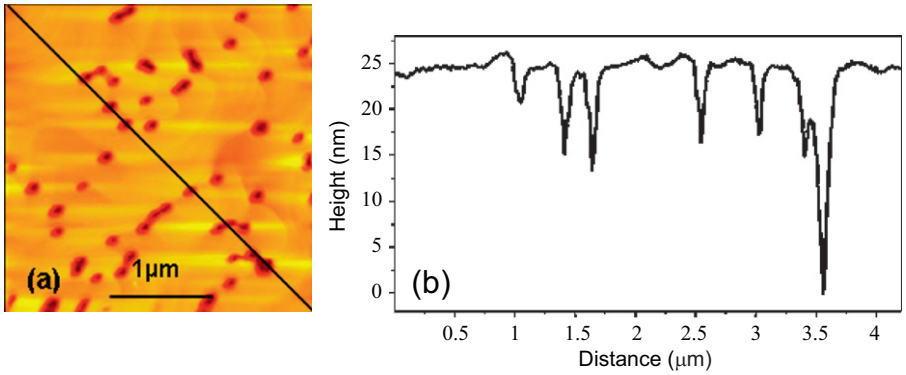

Fig. 2. (a) $3 \times 3\,\mu m^2$ surface AFM image and (b) cross-sectional scan of GaN buffer layer. The solid line on the 2D AFM image corresponds to the cross-sectional scan.

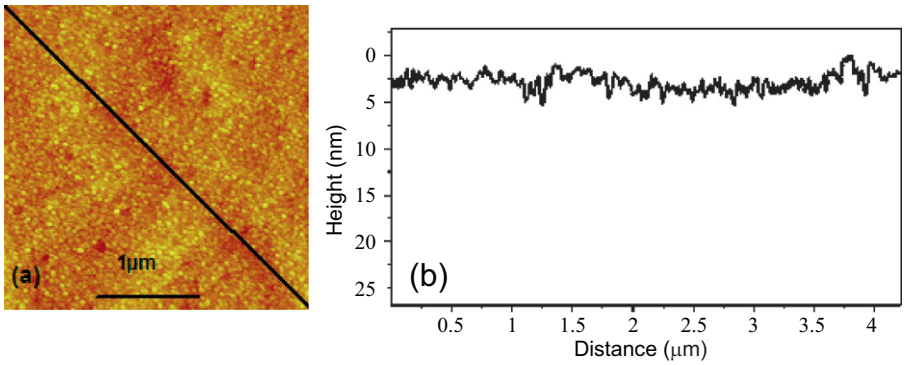

Fig. 3. (a) $3 \times 3\,\mu m^2$ surface AFM image and (b) cross-sectional scan of 50 nm thick $B_{0.027}Ga_{0.073}N$ film. The solid line on the 2D AFM image corresponds to the cross-sectional scan.

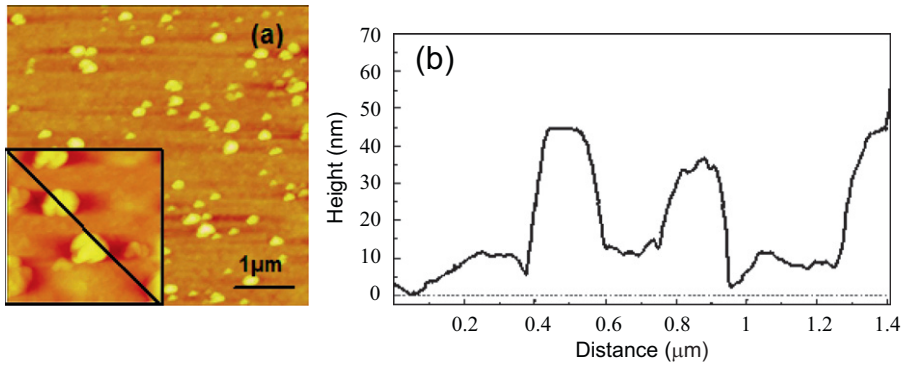

Fig. 4. The $5 \times 5\,\mu m^2$ and $1 \times 1\,\mu m^2$ (inset) 2D AFM topography and corresponding cross-sectional scan of 170 nm thick BGaN epilayer grown at the TEB/III ratio of 6%. The solid line on the 2D AFM image corresponds to the cross-sectional scan.

to this optimum thickness. This optimum thickness t_{sp}, which corresponds to the starting point of phase separation for a given TEB/III ratio, decreases as the TEB/III ratio increases.

Measurements of the composition for the surface and subsurface film levels were performed by XPS analysis prior and after sputtering, respectively. Typical XPS spectra are presented in Fig. 5 which exhibits the characteristic lines for all the basic elements of BGaN, i.e. gallium, boron, and nitrogen. Besides these peaks, oxygen and carbon were detected on the surface and the corresponding signal drops drastically after surface sputtering meaning that a large percentage of C and O concentrations is related to the surface contamination. The binding energy of the B 1s peak is located between 190.2 and 191.1 eV (insets in Fig. 5), in good agreement with the value of 190–191 eV given for B–N bonds [8,9]. The N 1s asymmetric peak with a shoulder at higher binding energy could be decomposed into two maxima centered at 397.0–398.1 eV and 400 eV, which are attributed to nitride and N–O bonds, respectively. The N 1s nitride single peak with peak position varying from 397.0 to 398.1 eV, depending on the boron content of the sample, is a characteristic signature of the BGaN ternary films with different boron concentrations. A similar feature was reported by Witthaut et al. [10] for BAlN material. In addition, for our BGaN samples, the sputtering treatment leads to a noticeable decrease in the intensity of the B 1s core level, and a shift of the nitride N 1s peak towards lower binding energy, i.e. the GaN peak position. These results, B 1s core intensity decrease and nitride N 1s peak shift, are strong indications of boron accumulation on the surface.

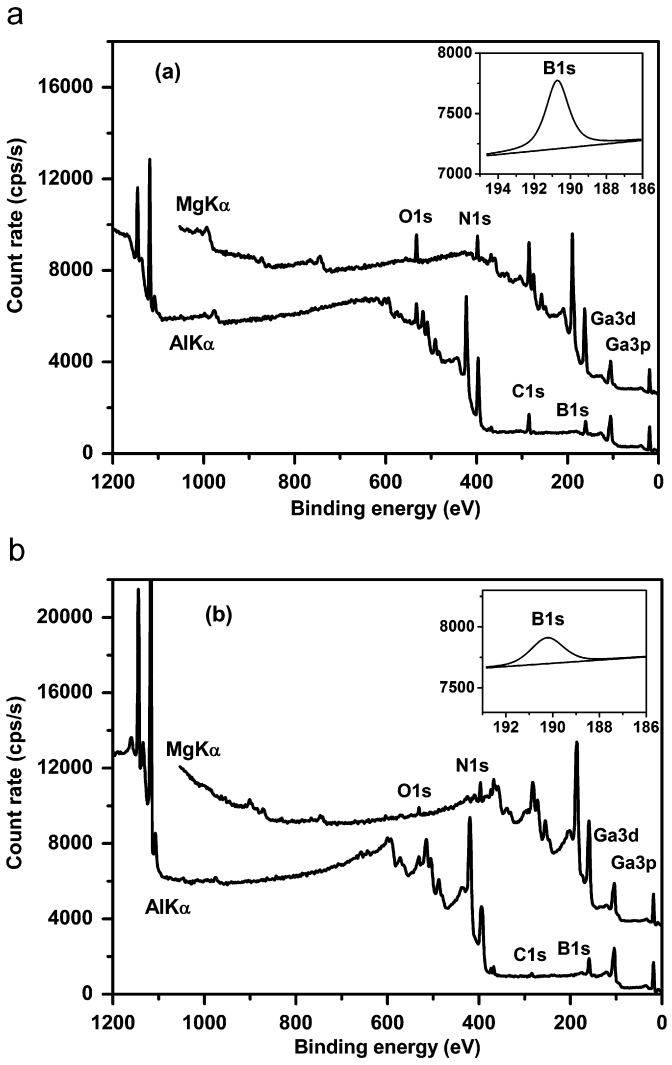

Fig. 5. Typical XPS spectra of BGaN film deposited for TEB/III ratio of 6% (a) before and (b) after surface sputtering. The insets compare the boron peaks evolution with sputtering.

Fig. 6 presents the $B_xGa_{1-x}N$ boron composition (%) versus TEB/III ratio (%) deduced from XPS and XRD analysis and the insets of Fig. 6 present corresponding SEM images. The boron composition deduced from XPS analysis after sputtering (triangles) varies linearly with the TEB/III ratio. These values are in a good agreement with the XRD measurements (circles). Furthermore, taking into account the accuracy of XPS, the boron surface composition (square marks) is higher than that in the subsurface and in the volume for any TEB/III ratio and the surface morphology. For 4% TEB/III ratio (175 nm) with a surface composed of small crystallites as well as for the 6% TEB/III ratio (250 nm) with a large crystallites surface morphology, the surface boron content is higher than that of the subsurface. This feature means that the boron surface segregation is not morphologically dependent. Moreover, the boron composition (deduced from XPS) of the as-grown surface (square marks) increases drastically from 3.6% to 8.9% for film thickness of 175 and 1000 nm, respectively. This means that the surface boron accumulation is higher with increasing thickness for the same TEB/III ratio. The combination of these two parameters, TEB/III ratio and thickness, can explain why the value of surface boron content obtained for 6% TEB/III ratio (250 nm) is higher than that for 8% TEB/III (120 nm).

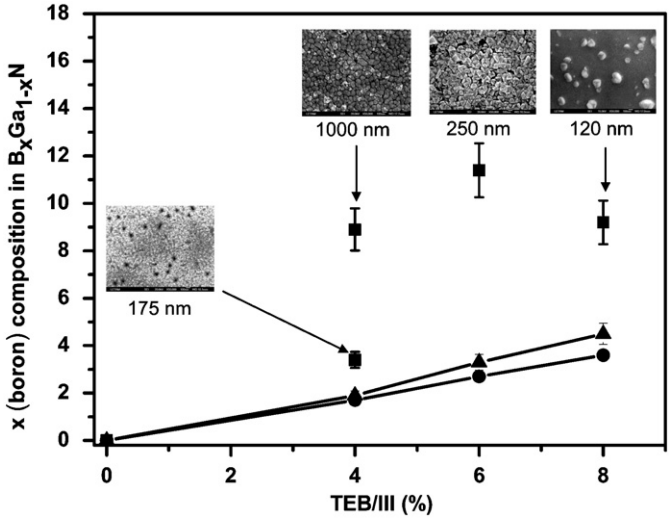

Fig. 6. $B_xGa_{1-x}N$ boron composition (%) versus TEB/III ratio deduced from XPS measurements before (squares) and after sputtering (triangles). Error bars represent the accuracy of the method (±10%). XRD data are shown with circles. The insets present BGaN surface morphology before sputtering.

We can deduce from our results that the phase separation occurs above an optimum thickness t_{sp}. Moreover, once a critical surface boron concentration is reached, phase separation occurs resulting in the change of the growth mechanism of BGaN. Indeed, the nucleation rate is modified with the supersaturation, adatom concentration, and adatom diffusion on the surface, as it has recently been reported for BAlN material [11]. As for BAlN alloy [11], boron surface segregation in BGaN affects the surface diffusion, the Ga and N adsorption, and the nucleation rates. We can conclude that these effects result in the nucleation and growth of subsequent second phase BGaN.

4. Conclusion

$B_xGa_{1-x}N$ materials were grown by LP-MOVPE for different thicknesses and TEB/III ratios. SEM and AFM observations clearly reveal the formation of large polygonal crystallites for TEB/III ratio and film thickness exceeding the optimum values. XPS measurements demonstrate that surface boron content is higher compared to that in the volume and it increases with the TEB/III ratio and the thickness. Moreover, surface accumulation of boron enhances the phase separation phenomenon. As a result, this effect limits the growth of uniform single phase BGaN. We have demonstrated the possibility to grow boron contained films $B_xGa_{1-x}N$/GaN/sapphire up to $x = 3.6\%$ of single phase by limiting the layer thickness ($< t_{sp}$). In addition, we have also proposed that below the t_{sp} thickness the small BGaN crystallites could play a role of barriers for threading dislocations.

References

[1] C.H. Wei, J.H. Edgar, J. Crystal Growth 217 (2000) 109.
[2] L.K. Teles, J. Furthmüller, L.M.R. Scofaro, A. Tabata, J.R. Leite, F. Bechsedt, T. Frey, D.J. As, K. Lischka, Physica E 13 (2002) 1086.
[3] A.Y. Polyakov, M. Shin, M. Skowronski, D.W. Greve, R.G. Wilson, A.V. Govorkov, R.M. Desrosiers, J. Electron. Mater. 26 (1997) 237.
[4] C.H. Wei, Z.Y. Xie, J.H. Edgar, K.C. Zeng, J.Y. Lin, H.X. Jiang, C. Ignatiev, J. Chaudhuri, D.N. Braski, MRS Int. J. Nitride Semicond. Res. 4S1 (1999) G 3.79.
[5] A. Ougazzaden, S. Gautier, C. Sartel, N. Maloufi, J. Martin, F. Jomard, J. Crystal Growth 298 (2007) 316.
[6] T. Akasaka, Y. Kobayashi, T. Makimoto, J. Crystal Growth 298 (2007) 320.

[7] S. Gautier, C. Sartel, S. Ould-Saad, J. Martin, A. Sirenko, A. Ougazzaden, J. Crystal Growth 298 (2007) 428.
[8] D.N. Hendrickson, J.M. Hollsnder, W.L. Jolly, Inorg. Chem. 9 (1970) 612.
[9] S. Kohiki, T. Ohmura, K. Kusao, J. Spectrosc. Relat. Phenom. 31 (1983) 85.
[10] M. Witthaut, R. Cremer, D. Neuschiitz, Surf. Interface Anal. 30 (2000) 580.
[11] M. Albrecht, J. Wollweber, M. Rossberg, M. Schmidbauer, C. Hartmann, R. Fornari, Appl. Phys. Lett. 88 (2006) 211904.